Dimension-Reduced Radio Astronomical Imaging Based on Sparse Reconstruction

Shuimei Zhang, Yujie Gu, Chang-Hee Won, and Yimin D. Zhang
Department of Electrical and Computer Engineering
Temple University, Philadelphia, PA 19122, USA

***Abstract*—Modern radio telescopes commonly use antenna arrays to achieve high-resolution imaging, and various beamforming techniques have been developed in radio astronomy to generate dirty images. Because the manifold of a radio telescope array varies over time due to Earth rotation, beamformers are separately designed and implemented at each time epoch, and the resulting images are averaged over multiple epochs to form enhanced dirty images. Because astronomical scenes are typically sparse, we propose a new method through sparse reconstruction to obtain clean astronomical images. To reduce the computational complexity, a singular value decomposition based compressive sensing scheme is applied. The proposed method offers reduced computational complexity while maintaining the high quality of the sparse reconstruction. Unlike traditional beamforming techniques which require an additional deconvolution procedure for clean image formation, the proposed technique provides clean astronomical images directly with accurate estimation of the source position and intensity.**

***Index Terms*—Compressive sensing, data fusion, dimension reduction, radio astronomical imaging.**

I. Introduction

Modern radio astronomical telescopes commonly use an array consisting of multiple antennas to construct astronomical images based on the principle of radio interferometry [1]. Radio astronomical images can be obtained using beamforming methods [2]–[5]. Among them, delay-and-sum (DAS) is a conventional data-independent beamformer, whereas minimum variance distortionless response (MVDR) [6] and adaptive angular response (AAR) [2] are adaptive beamforming techniques commonly used in radio astronomy. Because the manifold of radio telescope arrays varies over time due to Earth rotation, beamformers are separately designed and implemented at different time epochs during which the array manifold is considered unchanged. The resulting images obtained at these time epochs are then averaged to form enhanced images, typically over a multi-hour period [3]. Such images are commonly referred to as dirty images because of their limited image resolution determined by the array aperture. The corresponding clean images can be obtained through image deconvolution. Two deconvolution techniques, namely, the CLEAN method [7] and the maximum entropy method [8], are commonly used to reconstruct clean radio astronomical images.

Because astronomical objects are distantly separated, astronomical scenes are typically sparse. In radio astronomical imaging, the sparsity is further enhanced because signals at different frequency bands are separately processed. Therefore, sparse reconstruction techniques find useful in astronomical imaging in recent years [9]–[12]. However, in the literature, sparse reconstruction is only utilized for each time epoch. Few methods utilize coherent combining of the data observed over multiple time epochs to improve the image quality [13].

In this paper, we propose a new sparse reconstruction-based method to obtain clean astronomical images directly. In this method, the visibility data over different time epochs are fused to improve the robustness and quality of the resulting images. Data fusion is designed to effectively exploit the synthesized array aperture due to Earth rotation. Compared to beamforming-based techniques, data fusion is more important in sparse reconstruction-based methods because of the nonlinear thresholding implicitly implemented in their computations. This paper offers two major contributions, i.e., the fusion of the visibility data over multiple time epochs for imaging performance improvement, and the utilization of compressive sensing (CS) for computational complexity reduction. Note that, unlike traditional beamforming techniques which require an additional deconvolution step to generate clean images, the proposed technique provides clean astronomical images directly and enables accurate estimation of the source position and intensity.

Notations: We use lower-case (upper-case) bold characters to denote vectors (matrices). $\boldsymbol{I}_N$ denotes the $N \times N$ identity matrix. $(\cdot)^{\mathrm{T}}$ and $(\cdot)^{\mathrm{H}}$ denote the transpose and the Hermitian transpose of a matrix or a vector, respectively. $\mathrm{Diag}(\cdot)$ denotes a diagonal matrix with the elements of a vector as the diagonal entries, whereas $\mathrm{diag}(\cdot)$ denotes a vector consisting of the diagonal entries of a general matrix. $\mathrm{vec}(\cdot)$ converts a matrix to a vector by stacking the columns of the matrix one under the other.

II. System Model

In radio astronomy, we commonly use two coordinate systems, as shown in Fig. 1, respectively for the telescope array and the astronomical objects [14]. The vector baseline $\boldsymbol{d}_\lambda$ connects the two antennas in the (u, v, w) coordinate system, measured in wavelength. The component w is measured in the phase reference position direction $\boldsymbol{s}_0$, and components u and v are measured in a plane normal to the direction $\boldsymbol{s}_0$. The (ℓ, m) coordinate system corresponds to the projection

This work is supported in part by the National Science Foundation (NSF) under grant AST-1547420.

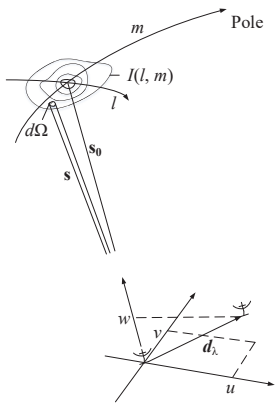

Fig. 1. Geometric relationship between a source under observation $I(\ell, m)$ and an interferometer or one antenna pair of an array.

of the celestial sphere onto a plane that is a tangent at the field center, measured in radians. Consider a radio telescope array consisting of P antennas, and astronomical sources are represented as D point sources in a specific observation area of interest. The source intensity is expressed as

$$I(\ell, m) = \sum_{d=1}^{D} I(\ell_d, m_d)\delta(\ell - \ell_d)\delta(m - m_d), \tag{1}$$

where $I(\ell_d, m_d), d = 1, \cdots, D$, denotes the source intensity at position (ℓ_d, m_d), and $\delta(\cdot)$ denotes the Dirac delta function.

Radio astronomical imaging is based on the visibility data, which is the correlation of the received array signals. Denote u_i^k and v_i^k as the baseline component at the i-th antenna and time epoch t_k. The visibility is expressed as $V(u, v)$, where $u \equiv u_{ij}^k = u_i^k - u_j^k$ and $v \equiv v_{ij}^k = v_i^k - v_j^k$ respectively stand for the baseline (between antennas i and j) in two orthogonal coordinate axes on the Earth surface as depicted in Fig. 1. Under certain standard approximations, such as planar arrays and small field of view imaging, the visibility and the astronomical source intensity for uncorrelated source points are associated with the two-dimensional Fourier transform, expressed as [3]

$$V(u_{ij}^k, v_{ij}^k) = \sum_{d=1}^{D} I(\ell_d, m_d) e^{-\jmath 2\pi(u_{ij}^k \ell_d + v_{ij}^k m_d)}, \tag{2}$$

where $\jmath = \sqrt{-1}$ is the imaginary unit. By selecting a reference point and denoting its coordinate as (u_0^k, v_0^k), we can reformulate (2) as

$$\begin{aligned} V(u_{ij}^k, v_{ij}^k) = &\sum_{d=1}^{D} e^{-\jmath 2\pi(u_{i,0}^k \ell_d + v_{i,0}^k m_d)} I(\ell_d, m_d) \\ &\cdot e^{\jmath 2\pi(u_{j,0}^k \ell_d + v_{j,0}^k m_d)}, \end{aligned} \tag{3}$$

which can be further expressed in a matrix form as

$$\boldsymbol{R}_k = \boldsymbol{A}_k \boldsymbol{B} \boldsymbol{A}_k^{\mathrm{H}}. \tag{4}$$

Here, $\boldsymbol{A}_k = [\boldsymbol{a}_k(\ell_1, m_1), \cdots, \boldsymbol{a}_k(\ell_D, m_D)]$ denotes the telescope array manifold matrix at time epoch t_k, where $\boldsymbol{a}_k(\ell_d, m_d) = [e^{-\jmath 2\pi(u_{1,0}^k \ell_d + v_{1,0}^k m_d)}, \cdots, e^{-\jmath 2\pi(u_{P,0}^k \ell_d + v_{P,0}^k m_d)}]^{\mathrm{T}}$ is the array steering vector of the d-th source and $\boldsymbol{B} = \mathrm{Diag}\,[I(\ell_1, m_1), \cdots, I(\ell_D, m_D)]$ is a diagonal matrix representing the intensity of point sources.

In practice, the array received signals are contaminated by additive system noise. Assuming independent and identically distributed (i.i.d.) additive white Gaussian noise at each antenna with noise power σ_n^2, the visibility matrix at time epoch t_k can be expressed as

$$\tilde{\boldsymbol{R}}_k = \boldsymbol{A}_k \boldsymbol{B} \boldsymbol{A}_k^{\mathrm{H}} + \sigma_n^2 \boldsymbol{I}_P. \tag{5}$$

III. Beamforming-based Radio Astronomical Imaging

Image formation is an inverse problem based on the visibility matrix observed at all baseline positions. A well-known classical imaging technique is the data-independent DAS beamformer, which computes the estimated source intensity at all positions within the interested region $\forall(\ell, m) \in \Omega$ as [3]

$$I^{\mathrm{DAS}}(\ell, m) = \frac{1}{K} \sum_{k=1}^{K} \boldsymbol{a}_k^{\mathrm{H}}(\ell, m) \tilde{\boldsymbol{R}}_k \boldsymbol{a}_k(\ell, m), \tag{6}$$

where K denotes the number of time epochs.

In order to improve the image resolution, a number of adaptive beamforming techniques have been developed for radio astronomical imaging. Two commonly used adaptive beamformers in radio astronomy are the MVDR beamformer [6], which is given as

$$I^{\mathrm{MVDR}}(\ell, m) = \sum_{k=1}^{K} \frac{1}{\boldsymbol{a}_k^{\mathrm{H}}(\ell, m) \tilde{\boldsymbol{R}}_k^{-1} \boldsymbol{a}_k(\ell, m)}, \tag{7}$$

and the AAR beamformer [2], which is expressed as

$$I^{\mathrm{AAR}}(\ell, m) = \frac{\sum_{k=1}^{K} \boldsymbol{a}_k^{\mathrm{H}}(\ell, m) \tilde{\boldsymbol{R}}_k^{-1} \boldsymbol{a}_k(\ell, m)}{\sum_{k=1}^{K} \boldsymbol{a}_k^{\mathrm{H}}(\ell, m) \tilde{\boldsymbol{R}}_k^{-2} \boldsymbol{a}_k(\ell, m)}. \tag{8}$$

For these beamforming-based techniques, the images are formed at each time epoch. The resulting images at different time epochs are then averaged over a long time period, typically in the order of hours, to form the final dirty image. A clean image with a higher resolution can be obtained by performing deconvolution to the dirty image.

IV. Proposed Method

Considering the fact that the sources are distant in the sky, astronomical images are sparse as most areas of the image are empty. In this section, we consider the image construction based on sparse reconstruction techniques. Fusion of the observed visibility data over different time epochs, and the utilization of the CS kernels based on the dictionary matrix are then discussed.

A. Sparse Image Reconstruction

Consider $\boldsymbol{b} = \text{diag}(\boldsymbol{B}) = [I(\ell_1, m_1), \cdots, I(\ell_D, m_D)]^{\text{T}}$ as a high-dimensional S-sparse vector. Vectorizing the covariance matrix $\tilde{\boldsymbol{R}}_k$ in (5) becomes

$$\tilde{\boldsymbol{r}}_k = \boldsymbol{r}_k + \sigma_n^2 \boldsymbol{i}, \tag{9}$$

where $\tilde{\boldsymbol{r}}_k = \text{vec}(\tilde{\boldsymbol{R}}_k)$, $\boldsymbol{r}_k = \text{vec}(\boldsymbol{A}_k \boldsymbol{B} \boldsymbol{A}_k^{\text{H}})$ and $\boldsymbol{i} = \text{vec}(\boldsymbol{I}_P)$. The reconstruction of the image vector $\boldsymbol{b}$ from the measured visibilities $\tilde{\boldsymbol{r}}_k$ can be formulated as a CS problem,

$$\tilde{\boldsymbol{r}}_k = \boldsymbol{\Phi}_k \boldsymbol{b} + \sigma_n^2 \boldsymbol{i}, \tag{10}$$

where $\boldsymbol{\Phi}_k \in \mathbb{C}^{P^2 \times D}$ is the dictionary matrix at time epoch t_k. Each column of the dictionary matrix is normalized.

This is a standard linear signal model used in CS and can be solved using many CS techniques, such as the orthogonal matching pursuit (OMP), least absolute shrinkage and selection operator (LASSO), and Bayesian sparse learning techniques [15]–[19]. However, the observation obtained at a single time epoch may not necessarily provide sufficient measurements to ensure robust imaging. To address this issue, we consider the data fusion over multiple time epochs in the following subsection.

B. Fusion of Multi-Epoch Visibility Data

The data observed at different time epochs correspond to the image scene with the same sparse support. Generally speaking, the raw data measured at different time epochs and different locations cannot be synchronously fused because of the different signal phases and propagation environments. For the underlying radio astronomical imaging, however, the values of $\boldsymbol{b}$ represent the power which are all positive and can be considered invariant with respect to different time epochs. We divide the entire observation time into several blocks, with each block including M time epochs. Then, stacking the visibility data observed at one block results in

$$\boldsymbol{x} = \begin{bmatrix} \tilde{\boldsymbol{r}}_1 \\ \tilde{\boldsymbol{r}}_2 \\ \vdots \\ \tilde{\boldsymbol{r}}_M \end{bmatrix} = \begin{bmatrix} \boldsymbol{\Phi}_1 \\ \boldsymbol{\Phi}_2 \\ \vdots \\ \boldsymbol{\Phi}_M \end{bmatrix} \boldsymbol{b} + \sigma_n^2 \begin{bmatrix} \boldsymbol{i} \\ \boldsymbol{i} \\ \vdots \\ \boldsymbol{i} \end{bmatrix}. \tag{11}$$

It is clear that the synthetic array baselines observed at different time epochs act as an equivalent array with an extended array aperture. Also, through the stacking of the vectorized visibility, the dimension of the measurement increases so that it helps to ensure the satisfaction of the restricted isometry property (RIP) condition for robust image construction [22].

C. Dimension-Reduced Sparse Reconstruction

Note that the dimension of the measurement $\boldsymbol{x}$ is determined by both the number of antennas P and the number of time epochs M. With the development of new radio telescopes such as the Square Kilometer Array (SKA) [20] and the Low-Frequency Array (LOFAR) [21], the number of antennas increases significantly. Hence, the computational complexity is a great concern because of the high-dimensional matrix operation. In order to reduce the complexity, a dimension-reduction scheme is utilized. Let $\boldsymbol{\Psi} \in \mathbb{C}^{N \times MP^2}$ $(N < MP^2)$ be a CS matrix consisting of N row-orthonormal sensing kernels, i.e, $\boldsymbol{\Psi}\boldsymbol{\Psi}^{\text{H}} = \boldsymbol{I}_N$. Applying $\boldsymbol{\Psi}$ to $\boldsymbol{x}$ in (11) yields,

$$\boldsymbol{y} = \boldsymbol{\Psi} \begin{bmatrix} \tilde{\boldsymbol{r}}_1 \\ \tilde{\boldsymbol{r}}_2 \\ \vdots \\ \tilde{\boldsymbol{r}}_M \end{bmatrix} = \boldsymbol{\Psi} \left(\begin{bmatrix} \boldsymbol{\Phi}_1 \\ \boldsymbol{\Phi}_2 \\ \vdots \\ \boldsymbol{\Phi}_M \end{bmatrix} \boldsymbol{b} + \sigma_n^2 \begin{bmatrix} \boldsymbol{i} \\ \boldsymbol{i} \\ \vdots \\ \boldsymbol{i} \end{bmatrix} \right). \tag{12}$$

As such, the stacked dictionary matrix is compressed from $\boldsymbol{\Phi} = [\boldsymbol{\Phi}_1^{\text{T}}, \cdots, \boldsymbol{\Phi}_M^{\text{T}}]^{\text{T}} \in \mathbb{C}^{MP^2 \times D}$ to $\boldsymbol{\Psi}\boldsymbol{\Phi} \in \mathbb{C}^{N \times D}$. Accordingly, the vectorized visibility vector $\boldsymbol{x} \in \mathbb{C}^{MP^2}$ is compressed to a measurement vector $\boldsymbol{y} \in \mathbb{C}^N$. The compression enables us to retrieve $\boldsymbol{b}$ from a lower-dimensional compressed measurement vector $\boldsymbol{y}$ in an efficient manner since the essential information contained in $\boldsymbol{x}$ is preserved.

Random sensing kernels such as Gaussian and Bernoulli kernels are commonly adopted in the CS literature [23], [24]. In these cases, the imaging quality suffers a signal-to-noise ratio (SNR) loss which is roughly proportional to the compression factor MP^2/N. In astronomical imaging, the signals are extremely weak; hence, we cannot afford significant power loss. Unlike random CS matrices, utilizing well-designed CS matrices may reduce the computational complexity without suffering the sparse reconstruction performance loss. Examples of such CS matrix design strategies include those based on singular value decomposition (SVD) [25] and maximum mutual information [26], [27].

In this paper, we notice the fact that the array manifold matrices for close time epochs are similar. In other words, there are high redundancies in $\boldsymbol{\Phi}$ so that its dimension can be reduced without losing useful information and energy. As such, we apply SVD on the stacked dictionary matrix $\boldsymbol{\Phi}$ to design the CS matrix. Decompose $\boldsymbol{\Phi}$ as

$$\boldsymbol{\Phi} = \boldsymbol{U}\boldsymbol{\Sigma}\boldsymbol{V}^{\text{H}}, \tag{13}$$

where $\boldsymbol{U}$ is an $MP^2 \times MP^2$ column-orthonormal matrix, $\boldsymbol{V}$ is a $D \times D$ column-orthonormal matrix, and $\boldsymbol{\Sigma}$ is an $MP^2 \times D$ matrix with singular values located in the diagonal. We select N principal singular values, and denote the corresponding N columns of $\boldsymbol{U}$ as $\bar{\boldsymbol{U}}$. Then, $\bar{\boldsymbol{U}}^H \in \mathbb{C}^{N \times MP^2}$ is taken as the CS matrix $\boldsymbol{\Psi}$. A rule of thumb is to retain enough singular values to make up 90% of the energy in $\boldsymbol{\Sigma}$. That is, the sum of the squares of the retained singular values should be at least 90% of the sum of the squares of all the singular values.

Take OMP as an example to perform sparse reconstruction. The computational complexity before the dimension reduction is $\mathcal{O}(SMP^2D)$, whereas after the dimension reduction becomes $\mathcal{O}(SND)$. Although SVD requires some extra computations, it is noted that such CS matrices are independent of the signal and are determined only by the array manifold matrices. Therefore, they can be precomputed off-line.

V. Simulation Results

In this section, we provide simulation results to demonstrate the performance of the proposed method and compare

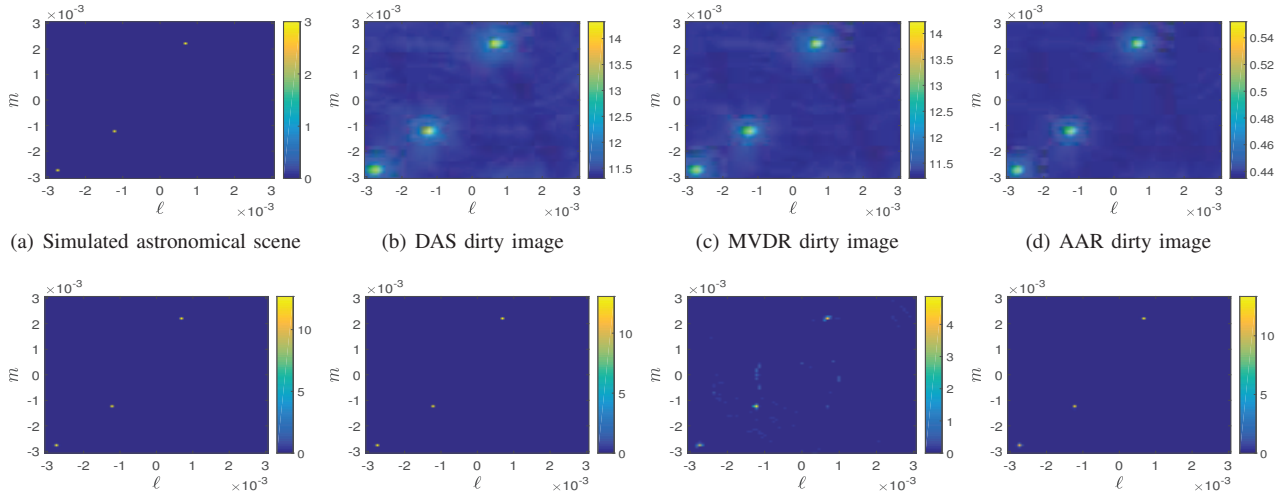

(a) Simulated astronomical scene (b) DAS dirty image (c) MVDR dirty image (d) AAR dirty image

(e) Method 1: OMP performed in each time epoch (f) Method 2: OMP performed in each block (no CS kernel) (g) Method 3: OMP performed in each block (random CS kernel) (h) Method 4: OMP performed in each block (SVD-based kernel)

Fig. 2. Comparison of imaging methods at SNR = -20 dB.

the results with traditional beamforming-based astronomical imaging methods including DAS, MVDR and AAR. As an example, the 27-element Very Large Array (VLA) [28] is considered with an observation time period of approximately 8 hours. The total number of time epochs is 690. The simulated astronomical region, shown in Fig. 2(a), contains a total number of $D = 81\times81 = 6,561$ pixels, and has three point sources present with the same intensity. The input SNR is defined as the power ratio between the average power of the three sources and the noise power. The row-orthogonal random CS kernels are drawn from an i.i.d. random Gaussian distribution $\mathcal{CN}(0,1)$. 90% of the energy is kept when designing the CS matrix utilizing the SVD of the stacked dictionary matrix.

To verify the effectiveness of the proposed imaging method in a low SNR environment, we set the SNR to be -20 dB. The simulation results are shown in Fig. 2. All three sources could be detected by different imaging methods. However, for beamforming-based imaging methods, the three sources in the dirty images shown in Figs. 2(b)–2(d) are smeared and corrupted by a high level of sidelobes.

For the sparse reconstruction-based imaging techniques, four different implementation methods are considered. For Method 1, sparse image reconstruction is taken place using a single-epoch measured data, and the resulting images are averaged over all the epochs. Methods 2, 3 and 4 exploit M epochs in each image reconstruction, and the final image is generated by averaging all the blocks. More specifically, Method 2 implements (11) without CS kernel, Method 3 implements (12) with Gaussian random projections, whereas Method 4 implements (12) with the designed SVD-based CS kernel. In all simulations, $M = 10$ is assumed.

The result of a single-epoch image is shown in Fig. 2(e), where several insignificant sporadic false positives around true point sources are observed. The images produced with multi-time-epoch data are shown in Figs. 2(f)–2(h). In Fig. 2(f), less false positives appear compared to Fig. 2(e). In Fig. 2(g), the compressive ratio is set as 5, whereas in Fig. 2(h) the average compressive ratio is approximately 20 and the obtained performance is similar to that in Fig. 2(f). We can conclude that the designed CS matrix achieves comparable performance with a significantly reduced computational complexity.

To quantitatively assess the imaging performance, we adopt the structural similarity (SSIM) index [29] as the evaluation criterion. From the comparison summarized in Table I we observe that Method 2 performs better than Method 1, thereby verifying the fact that data fusion of multiple time epochs can improve the sparse reconstruction performance. The imaging performance gap between Method 1 and Method 2 becomes more apparent for lower SNR values. Method 3, which exploits a random CS kernel, offers the worst imaging performance due to the SNR loss, whereas Method 4 (the proposed method) achieves a comparable performance to Method 2 since the designed CS matrix keeps most of the energy.

TABLE I
IMAGING QUALITY COMPARISON WITH DIFFERENT SNR LEVELS

SNR(dB)	Method 1	Method 2	Method 3	Method 4
-25	0.69	0.86	0.60	0.70
-20	0.96	0.97	0.68	0.96
-15	0.99	0.99	0.99	0.98

VI. CONCLUSION

In this paper, we proposed a new astronomical imaging method based on sparse reconstruction. The effectiveness of the proposed method was validated by simulation results with the VLA being considered as an example. Compared with the beamforming-based astronomical imaging methods, the proposed technique provides high-fidelity image reconstruction and power estimation. Fusion of measured data over multiple time epochs is effective in improving the reconstructed astronomical images. Also, the SVD-based CS matrix significantly reduces the computational complexity without compromising the performance of sparse image reconstruction.

REFERENCES

[1] M. Ryle, "A new radio interferometer and its application to the observation of weak stars," *Proc. Royal Society A*, vol. 211, pp. 351–375, 1952.

[2] C. Ben-David and A. Leshem, "Parametric high resolution techniques for radio astronomical imaging," *IEEE J. Sel. Topics Signal Process.*, vol. 2, pp. 670–684, Oct. 2008.

[3] R. Levanda and A. Leshem, "Synthetic aperture radio telescopes," *IEEE Signal Process. Mag.*, vol. 27, no. 1, pp. 14–29, Jan. 2010.

[4] Y. Gu and A. Leshem, "Robust adaptive beamforming based on interference covariance matrix reconstruction and steering vector estimation," *IEEE Trans. Signal Process.*, vol. 60, no. 7, pp. 3881–3885, July 2012.

[5] S. Zhang, Y. Gu, B. Wang and Y. D. Zhang, "Robust astronomical imaging under coexistence with wireless communications," in *Proc. Asilomar Conf. Signals, Systems, and Computers*, Pacific Grove, CA, Nov. 2017.

[6] A.-J. van der Veen, A. Leshem, and A.-J. Boonstra, "Signal processing for radio astronomical arrays," in *Proc. IEEE Sensor Array and Multichannel Signal Processing Workshop*, Barcelona, Spain, July 2004, pp. 1–10.

[7] J. A. Högbom, "Aperture synthesis with nonregular distribution of intereferometer baselines," *Astron. Astrophys. Suppl.*, vol. 15, pp. 417–426, June 1974.

[8] E. T. Jaynes, "Information theory and statistical mechanics," *Physical Rev.*, vol. 106, no. 4, pp. 620–630, 1957.

[9] Y. Wiaux, L. Jacques, G. Puy, A. Scaife, and P. Vandergheynst, "Compressed sensing imaging techniques for radio interferometry," *Mon. Not. R. Astron. Soc,*, vol. 395, no. 3, pp. 1733–1742, May 2009.

[10] R. E. Carrilo, J. D. McEwen, and Y. Wiaux, "Sparsity averaging reweighted analysis (SARA): a novel algorithm for radio interferometric imaging," *Mon. Not. R. Astron. Soc,* vol. 426, no. 2, pp. 1223–1234, Oct. 2012.

[11] H. Garsden et al., "LOFAR sparse image reconstruction," *Astron. Astrophys.,* vol. 575, no. A90, pp. 1–18, Mar. 2015.

[12] L. Wei, S. J. Wijnholds, and P. Hurley, "Robust recovery for aperture synthesis imaging," in *Proc. IEEE ICIP*, Beijing, China, Sept. 2017, pp. 3570–3574.

[13] S. Zhang, Y. Gu, W. C. Barott, and Y. D. Zhang, "Improved radio astronomical imaging based on sparse reconstruction," in *Proc. SPIE Compressive Sensing Conf.*, Orlando, FL, April 2018.

[14] A. R. Thomposon, J. M. Moran, and G. W. Swenson, *Interferometry and Aperture Synthesis in Radio Astronomy, 2nd Ed.* New York, NY: Wiley, 1986.

[15] J. A. Tropp and A. C. Gilbert, "Signal recovery from random measurements via orthogonal matching pursuit," *IEEE Trans. Inf. Theory*, vol. 53, no. 12, pp. 4655–4666, Dec. 2007.

[16] R. J. Tibshirani, "Regression shrinkage and selection via the LASSO," *J. Royal Statistical Society*, no. 1, vol. 58, pp. 267–288, 1996.

[17] S. Ji, Y. Xue, and L. Carin, "Bayesian compressive sensing," *IEEE Trans. Signal Process.*, vol. 56, no. 6, pp. 2346–2356, Jun. 2008.

[18] S. Ji, D. Dunson, and L. Carin, "Multi-task compressive sampling," *IEEE Trans. Signal Process.*, vol. 57, no. 1, pp. 92–106, Jan. 2009.

[19] Q. Wu, Y. D. Zhang, M. G. Amin, and B. Himed, "Complex multitask Bayesian compressive sensing," in *Proc. IEEE ICASSP*, Florence, Italy, May 2014, pp. 3375–3379.

[20] Square Kilometer Array (SKA) website: http://skatelescope.org

[21] Low-Frequency Array (LOFAR) website: https://www.lofar.org

[22] R. Baraniuk, "Compressive sensing," *IEEE Signal Process. Mag.*, vol. 24, no. 4, pp. 118–121, July. 2007.

[23] Y. Gu, C. Zhou, N. A. Goodman, W.-Z. Song, and Z. Shi, "Coprime array adaptive beamforming based on compressive sensing virtual array signal," in *Proc. IEEE ICASSP*, Shanghai, China, Mar. 2016.

[24] C. Zhou, Y. Gu, Y. D. Zhang, Z. Zhi, T. Jin, and X. Wu, "Compressive sensing based coprime array direction-of-arrival estimation," *IET Commun.,* vol. 11, no. 11, pp. 1719–1724, Aug. 2017.

[25] S. Zhang, Y. Zhu, and G. Kuang, "Truncated SVD-based compressive sensing for downward-looking three-dimensional SAR imaging with uniform/nouniform linear array," *IEEE Geosci. Remote Sens. Lett.*, vol. 12, no. 9, pp. 1853–1857, Sep. 2015.

[26] Y. Gu, Y. D. Zhang, and N. A. Goodman, "Optimized compressive sensing-based direction-of-arrival estimation in massive MIMO," in *Proc. IEEE ICASSP*, New Orleans, LA, Mar. 2017.

[27] Y. Gu and N. A. Goodman, "Information-theoretic compressive sensing kernel optimization and Bayesian Cramér-Rao bound for time delay estimation," *IEEE Trans. Signal Process.*, vol. 65, no. 17, pp. 4525–4537, Sept. 2017.

[28] Very Large Array (VLA) website: http://www.vla.nrao.edu

[29] Z. Wang, A. C. Bovik, H. R. Sheikh, and E. P. Simoncelli, "Image quality assessment: From error visibility to structural similarity," *IEEE Trans. Image Process.*, vol. 13, no. 4, pp. 600–612, Apr. 2004.